Optimizing Statistical Field Uniformity for RF Heating in Lyophilization: Modeling and Experimental Validation

Ahmad Darwish, *Member, IEEE*, Andrew David Strongrich, Alina Alexeenko, and Dimitrios Peroulis, *Fellow, IEEE*

***Abstract*— Freeze-drying has been widely adopted in the manufacturing of biologics for producing vaccines and protein-based therapeutics that are highly unstable in liquid form. Radio-frequency-assisted lyophilization (RFAL) can significantly accelerate drying by applying highly controllable volumetric heating. In this article, we design, for the first time, a quasi-random field (qRF) system. The system demonstrates: 1) primary drying acceleration and 2) very high uniformity with two different types of antennas at 8 GHz. Specifically, a double-ridged horn antenna and a wideband conical antenna are designed and placed inside a metallic enclosure [reverberation chamber (RC)] to excite electromagnetic waves inside a standard R&D freeze-dryer. The most suitable antenna type and location are determined using full-wave simulations. Compared with the standard 2.45 GHz frequency of operation, the electromagnetic field uniformity is improved by 2.47 times at 8 GHz. Furthermore, we show a primary drying acceleration of 81% with the wideband conical antenna and 119% with the double-ridged horn antenna using only 25 W of RF power. Residual moisture content measurements validate the proposed design for both implementations.**

***Index Terms*— Antenna, electromagnetic field uniformity, lyophilization, radio frequency (RF) heating, RF-assisted freeze-drying.**

I. Introduction

BIOPHARMACEUTICAL lyophilization, or freeze-drying, has become an indispensable process since World War II due to the high demand for blood plasma, vaccine, and drug products' stabilization [1], [2], [3]. While such a demand has consistently been increasing over the past 30 years due to the rapid development of biopharmaceuticals (especially in sensors' technologies and automation), the COVID-19 pandemic has put lyophilized products in the daily news since 2020 [4], [5], [6], [7], [8]. Toward that end, such a process has been extensively used to overcome the instability barrier of vaccines and protein-based therapeutics that are highly unstable in liquid form. As of 2018, formulations of about 30% of the approved parenteral protein by the European medicines agency were lyophilized products [9], [10]. Nonetheless, despite its advantages, lyophilization is among the most industrial energy and capital-intensive processes, prohibiting the attainment of an optimized, flexible manufacturing process [11], [12]. Conventional lyophilization involves placing frozen or aqueous products on temperature-controlled shelves inside a vacuum-controlled freeze-dryer. The product undergoes four primary stages, i.e., pretreatment, freezing, primary drying (sublimation drying), and secondary drying [13], [14]. Primary drying is typically described as the longest and most time-consuming stage. Therefore, microwave/radio frequency (RF) freeze-drying has been used as an alternative to the conventional counterpart to accelerate the process and reduce energy consumption [4], [15].

Unlike conventional freeze-drying, which involves conduction and convection heating mechanisms through indirect heat transfer with a cold fluid (refrigerant fluid), RF-assisted lyophilization (RFAL) uses high-frequency electromagnetic waves to target the frozen water at a molecular level. Hence, the removal of ice content is faster (volumetric heating). The use of RFAL allows many of the shortcomings associated with conventional freeze-drying to be avoided by simultaneously reducing the primary drying time while facilitating the integration of closed-loop control and improving the field uniformity [4], [9], [16], [17].

Numerous studies on RFAL have been introduced over the past few decades. Copson initially introduced RF heating in the food industry [18]. Nonetheless, limited studies have integrated microwaves and RF systems with the lyophilization of biopharmaceutical products. Dolan [19] demonstrated the feasibility of lyophilization of aqueous materials with the help of RF heating. Wang and Chen [20] conducted experimental and theoretical investigations on the impact of using dielectric material (Sintered SiC) in RFAL. The primary drying time was reduced by more than 20% when RFAL was used. A methodological use of experimental planning for the optimization of the drying of enzymes was carried out in [21] with the aim of developing a better understanding of RF integration with lyophilization. The impact of chamber pressure and input power on the enzymatic and water activity of the product was investigated. The study showed that high power and vacuum pressure reduced the primary drying time.

Manuscript received 30 October 2023; revised 29 February 2024; accepted 7 March 2024. Date of publication 25 March 2024; date of current version 4 April 2024. This work was supported by the National Institute for Innovation in Manufacturing Biopharmaceuticals (NIIMBL) through the Project Award Agreement. The Associate Editor coordinating the review process was Dr. Yang Bai. *(Corresponding author: Ahmad Darwish.)*

Ahmad Darwish and Dimitrios Peroulis are with the School of Electrical and Computer Engineering and Birck Nanotechnology Center, Purdue University, West Lafayette, IN 47907 USA (e-mail: andarwis@purdue.edu; dperouli@purdue.edu).

Andrew David Strongrich is with the School of Chemical Engineering and Birck Nanotechnology Center, Purdue University, West Lafayette, IN 47907 USA (e-mail: astrongr@purdue.edu).

Alina Alexeenko is with the School of Chemical Engineering, Aeronautics and Astronautics, and Birck Nanotechnology Center, Purdue University, West Lafayette, IN 47907 USA (e-mail: alexeenk@purdue.edu).

Digital Object Identifier 10.1109/TIM.2024.3381275

Further development on RFAL was carried out by Gitter et al. [9], [22]. Most existing studies until 2019 relied on using magnetrons as the source of RF power. However, the use of such sources led to inferior batch homogeneity when compared with conventional freeze-drying (measured through residual moisture distribution). Toward that end, a solid-state RF generator has been used to address the homogeneity issue in [9]. The obtained results showed a batch homogeneity comparable to that of conventional freeze-drying. Bhambhani et al. [12] applied RFAL (using up to 1200-W RF power) to vaccine samples and showed a significant time reduction on the primary drying while maintaining products' activity and stability. Our study demonstrates that a higher RF frequency (8 GHz) provides much-improved batch homogeneity. Using a double-ridged horn antenna, we accelerate primary drying by 119% with only 25 W of RF power. A wideband conical antenna results in an acceleration of 81%.

Abdelraheem et al. [4], [23] proposed the first systematic approach for designing a metallic chamber used in RFAL based on the statistical electromagnetic (SEM) theory. In this work, we use full-wave finite element (FE) modeling to further improve the design of such chambers. We demonstrate that the electromagnetic field uniformity is highly dependent on the radiator type, whereas the average electric field intensity depends on the location and type of radiator. Using a unidirectional antenna (horn antenna) allows the electromagnetic waves to be scattered by the mechanical stirrers before reaching the products. Thus, the electromagnetic field uniformity and batch homogeneity are improved. On the other hand, an omnidirectional antenna (a conical antenna) exposes some products to high RF power density compared with others before being scattered by the stirrers. The average electric field intensity increased by 1.29 times by changing the horn antenna location, whereas the field homogeneity increased by 1.25 times using the horn antenna when compared with the conical antenna (for an empty cavity). Experimental validation is carried out by monitoring two products' temperatures and evaluating the residual moisture content of selected freeze-dried products. The higher average electric field intensity and improved uniformity of the horn antenna resulted in a significantly improved freeze-drying cycle time and batch homogeneity.

II. FE-Based SEMs, RF Chamber, and Used Antenna

The classical SEM theory addresses electromagnetic interference in electrically large, complex, and irregular enclosures, generating multiple coexisting modes inside the cavity. SEM is widely used to overcome the time-consuming or impractical process of obtaining explicit analytical solutions for the electromagnetic field distribution inside the cavity [24]. Since RFAL involves electrically large cavities, SEM theory can be applied to design and optimize such RF chambers. The SEM theory and its application to RFAL are thoroughly discussed in [4]. FE-based analysis can be used to further simplify the SEM analysis for the design of lyophilization chambers.

The RF chamber, also known as the reverberation chamber (RC), comprises the first component implemented and

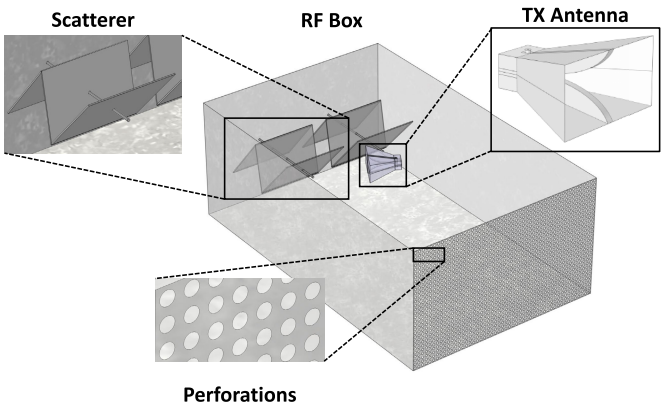

(a)

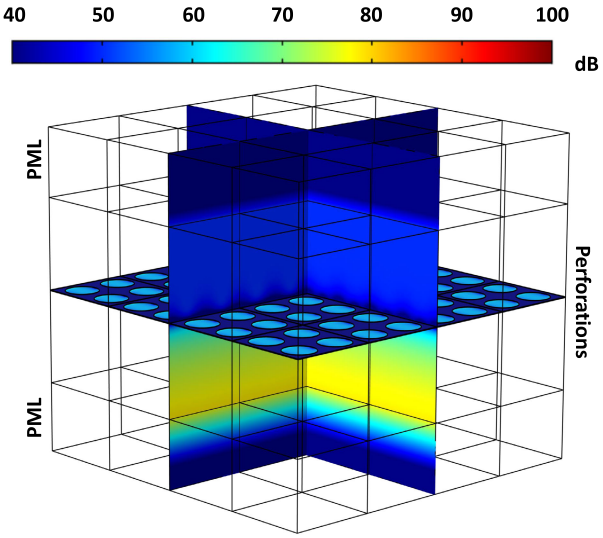

(b)

Fig. 1. Chamber and antenna design. (a) Designed RC: the antenna is hanging from the ceiling of the chamber. Two mechanical stirrers are placed on one side of the RC due to the constrained space inside the freeze-dryer. Perforations are designed to keep most of the RF energy stored inside the chamber, as depicted by (b). Simulated shielding effectiveness of 26.7 dB has been assessed at 8 GHz.

designed. Larger RCs are desirable to maximize the product volume while minimizing manufacturing costs. For a given RF frequency, a larger RC also increases the number of coexistent modes inside the chamber, improving the electromagnetic field uniformity [25], [26]. In this study, however, we are restricted to a laboratory-scale lyophilizer for conducting RFAL experiments. This limits the maximum possible size of the RC to $150 \times 250 \times 400$ mm.

Since the primary drying and secondary drying stages of the freeze-drying involve release of water vapor, which is a direct result of sublimation, we cannot use a fully encapsulated metallic enclosure as our RC. Hence, perforations with 1.5 mm radii are added across one side of the chamber, as shown in Fig. 1(a). The simulation results show that such perforations produce a shielding effectiveness of 26.7 dB at 8 GHz. The differential quality factor approach discussed in [4] validated that the chosen perforations provide high

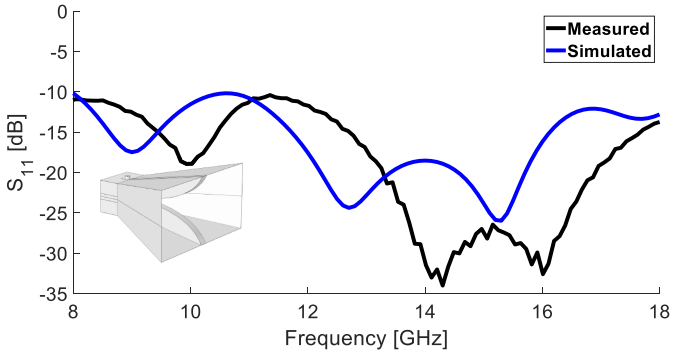

(a)

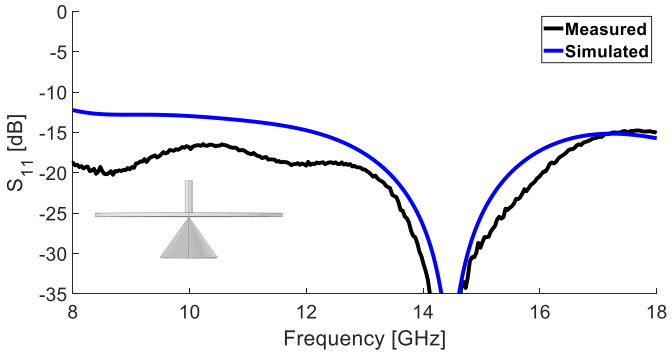

(b)

Fig. 2. Measured reflection coefficients (S_{11}) of (a) double-ridged horn antenna and (b) conical antenna. Both the antennas exhibit a large bandwidth covering the full intended range (8–18 GHz). The largest dimensions of the horn and conical antennas are 51 and 50 mm, respectively.

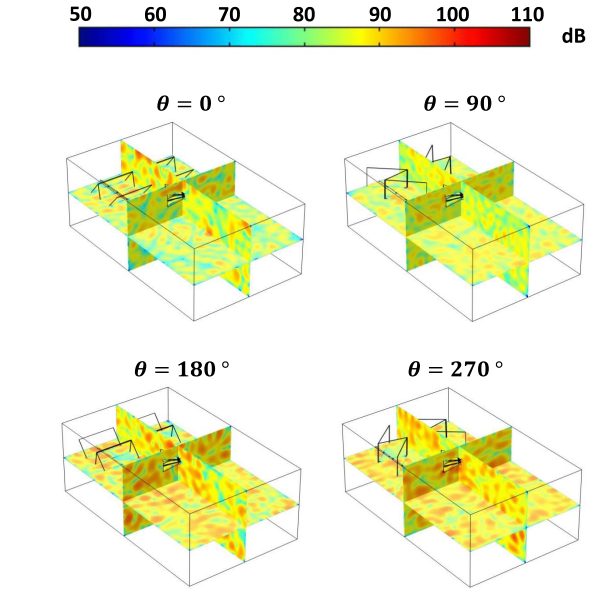

(a)

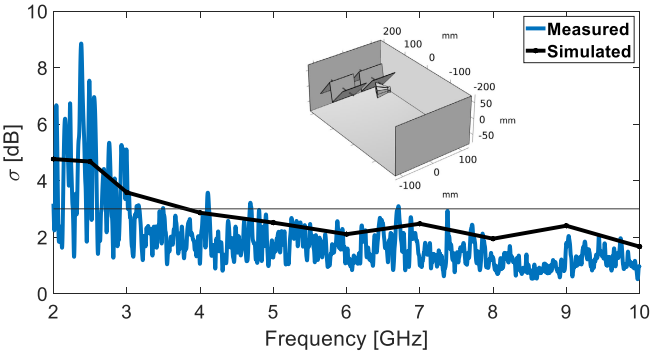

(b)

Fig. 3. (a) Simulated logarithmic scale of the electric field intensity inside the RC for different stirring angles (8 GHz). Different electric field distributions are achieved, verifying the effectiveness of the designed stirrers. The input power to the antenna is set to 75 W. (b) Electromagnetic field nonuniformity plot. Based on the observed results, the statistical field nonuniformity becomes independent of frequency above 8 GHz.

shielding effectiveness. Sixty-four perforations with a height of 1 mm are modeled, as depicted in Fig. 1(b). A perfect electric conductor (PEC) boundary condition models all the metallic parts to reduce the computational time. A periodic boundary condition models an infinite sheet with perforations. A perfectly matched layer (PML), with the PML wavelength set to account for the angular dependence of the normal component of the wave vector, is applied to model an open space above and below the perforations [27].

We have designed the two RF antennas (a double-ridged horn antenna and a wideband conical antenna) using a commercial full-wave simulator (COMSOL) to optimize the bandwidth and gain of the antennas. The obtained results are experimentally validated, as depicted in Fig. 2. The two antennas are selected because they exhibit a wideband operation (8–18 GHz), handle high RF power, and require a small size inside the RF chamber. Although the experiments carried out in this article are limited to 8 GHz, the wideband property of the antennas is desired for future integration with closed-loop control systems. On the other hand, two mechanical stirrers change the electromagnetic field distribution inside the chamber. The stirrers are identical and are placed at one end of the chamber, as shown in Fig. 1(a). The freeze-dryer used to conduct the experiments imposes the location of the designed stirrers (due to space restriction). The largest dimension of the stirrers is 11.5 cm, whereas the smallest is 8 cm to meet the IEC 61000-4-21 standards, given by [28]

$$L_{\text{stir}} \geq \frac{\lambda_{\text{LUF}}}{4} \tag{1}$$

$$L_{\text{stir}} \geq \frac{3\min(a, b, c)}{4} \tag{2}$$

where L_{stir} represents the largest dimension of the stirrers, λ_{LUF} is the wavelength of the lowest usable frequency, and a, b, and c are the dimensions of the RC.

After implementing the chamber, the antenna, and the stirrers, we obtain the SEM field intensity and uniformity using FE modeling [4], [29]. Initially, we acquire the magnitude of the three electric field components at 1386 sensing points distributed uniformly inside the RC as the mechanical stirrers are rotated. Then, the average electric field magnitude at every

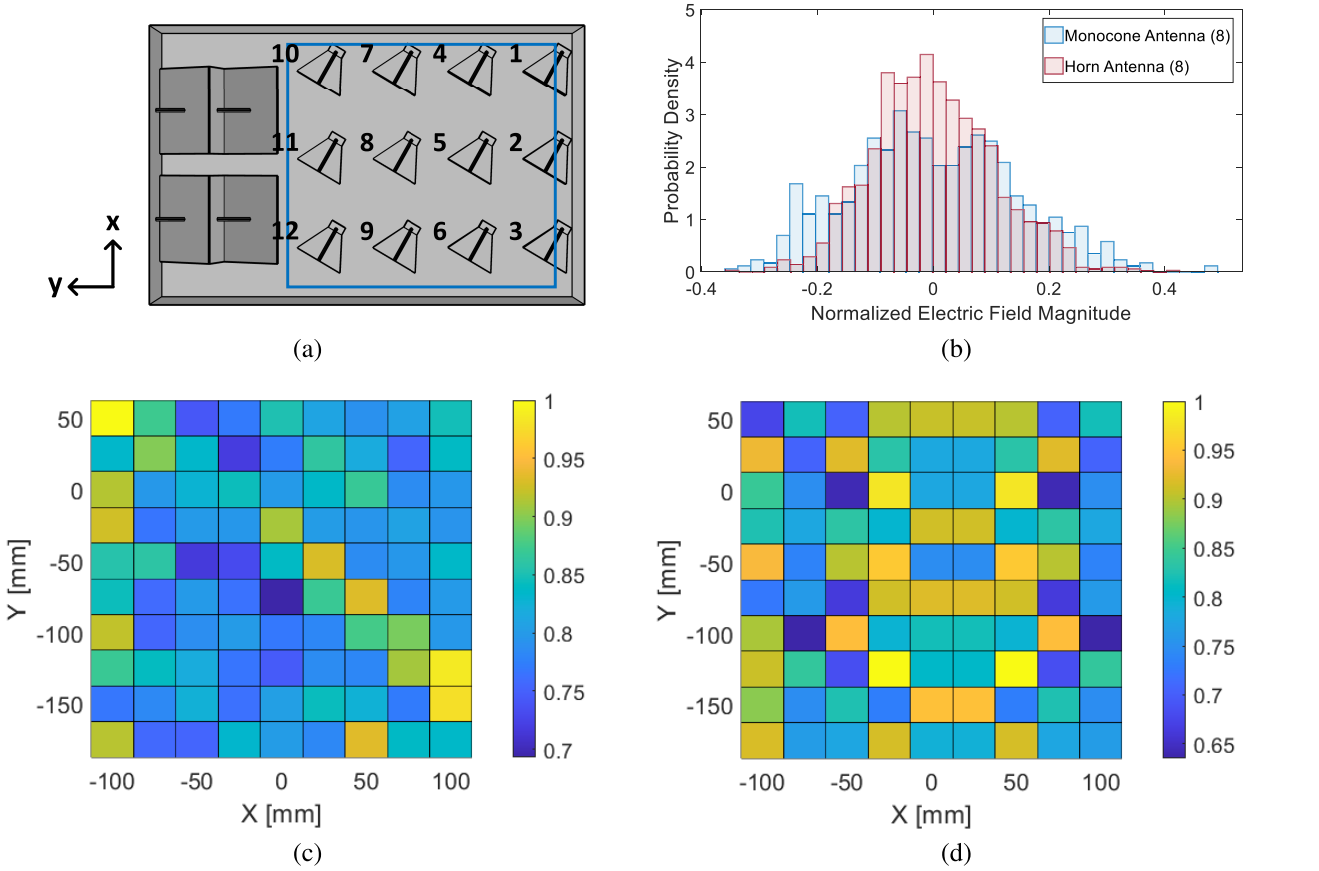

Fig. 4. SEM field uniformity. (a) Twelve positions at which the antenna has been placed to obtain the SEM metrics. (b) Normalized histogram that shows the probability density distribution for the conical (monocone) antenna and the double-ridged horn antenna (at position 8). (c) Spatial distribution of the electric field inside the RC using the double-ridged horn antenna. (d) Spatial distribution of the electric field inside the RC using the conical antenna. The average intensity of the field inside the chamber due to the double-ridged horn antenna is higher than that of the conical antenna due to the lower reflections absorbed by the horn antenna.

TABLE I
SIMULATED STATISTICAL ELECTRIC FIELD UNIFORMITY INSIDE THE RC

Antenna Type (Position)	$\langle \mathbf{E} \rangle$ (kV/m)	σ (dB)
Monocone (8)	6.14	2.36
Horn (1)	8.56	1.92
Horn (2)	8.50	1.90
Horn (3)	6.77	1.95
Horn (4)	8.32	1.94
Horn (5)	8.71	1.89
Horn (6)	7.97	1.97
Horn (7)	8.26	1.99
Horn (8)	8.68	1.94
Horn (9)	7.77	1.92
Horn (10)	7.99	1.96
Horn (11)	7.56	1.94
Horn (12)	7.48	1.96

sensing point is evaluated using

$$\langle E_x \rangle = \frac{\sum_{k=1}^{90} E_{x,k}}{90} \tag{3a}$$

$$\langle E_y \rangle = \frac{\sum_{k=1}^{90} E_{y,k}}{90} \tag{3b}$$

$$\langle E_z \rangle = \frac{\sum_{k=1}^{90} E_{z,k}}{90} \tag{3c}$$

where k represents the number of stirring angles to complete a full revolution (steps of 4°). The stirrers alter the distribution of the electric field inside the RC at each stirring angle, as depicted by Fig. 3(a). Next, the average electric field components over the entire RC volume (using the 1386 sensing points) are evaluated as follows:

$$\langle \mathbf{E_x} \rangle = \frac{\sum_{m=1}^{1386} \langle E_x \rangle_m}{1386} \tag{4a}$$

$$\langle \mathbf{E_y} \rangle = \frac{\sum_{m=1}^{1386} \langle E_x \rangle_m}{1386} \tag{4b}$$

$$\langle \mathbf{E_z} \rangle = \frac{\sum_{m=1}^{1386} \langle E_x \rangle_m}{1386}. \tag{4c}$$

The total average electric field is then obtained using

$$\langle \mathbf{E} \rangle = \frac{\langle \mathbf{E_x} \rangle + \langle \mathbf{E_y} \rangle + \langle \mathbf{E_z} \rangle}{3} \tag{5}$$

and the standard deviation (dB) is evaluated by

$$\sigma_{\text{dB}} = 20 \log_{10} \frac{\sigma_{\text{Linear}} + \langle \mathbf{E} \rangle}{\langle \mathbf{E} \rangle} \tag{6}$$

where σ_{Linear} is the standard deviation of the total average electric field

$$\sigma^2_{\text{Linear}} = \frac{\sum_{n=1}^{1386} \sum_{p=x,y,z} (\langle E_p \rangle_n - \langle \mathbf{E} \rangle)^2}{4158 - 1}. \tag{7}$$

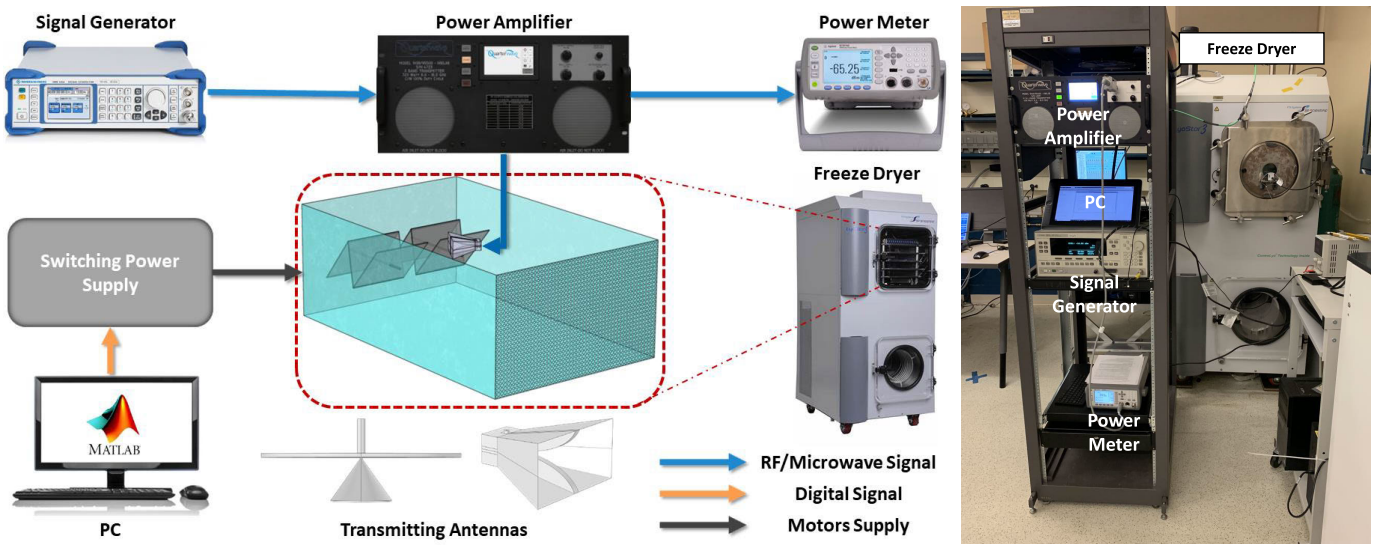

Fig. 5. RFAL system configuration and experimental setup.

Fig. 6. Karl Fischer moisture analyzer used to obtain the residual moisture content.

The electric field uniformity is initially obtained to determine the minimum frequency that guarantees a standard deviation $\leq$3 dB (as per the IEC 61000-4-21 standard). This condition is met at frequencies above 7 GHz, as demonstrated experimentally in Fig. 3(b) [23]. A detailed description of the experimental measurements for the electromagnetic field is given in our previous work [23]. In Section IV, we show that higher frequencies improve the drying time of the lyophilized products. Therefore, all the simulation models are tested at 8 GHz to ensure that the standard deviation is below 3 dB while requiring a relatively low computational time compared with higher frequencies.

Next, the best position for the antenna is selected based on the obtained SEM parameters, i.e., average electric field intensity and uniformity. In [30], we have shown that a wide range of angular positions (using the double-ridged horn antenna) provides a high uniformity. Nonetheless, the angular position of 60° provides the highest average intensity since it reduces the reflected waves received by the antenna. We demonstrate in this work, using 12 simulation models, that the SEM metrics are highly dependent on the antenna position inside the RF chamber. Table I summarizes the simulated average electric field intensity and uniformity obtained by varying the location of the antenna (Fig. 4(a) shows the different antenna locations). In the unloaded condition, we observe that the two statistical metrics are improved when the double-ridged horn antenna is used (when compared with the conical antenna).

When the horn antenna is considered, the electromagnetic field intensity is the only factor dependent on its position (σ_{dB} variations are negligible, as depicted in Table I). Placing the antenna near the mechanical stirrers (positions 10, 11, and 12) or close to the metallic side of the chamber (positions 3, 6, and 9) increases the reflected RF signal to the radiator, reducing the average electric field intensity. On the other hand, placing the antenna at positions 1, 2, 4, and 7 increases the power density received by some products relative to others, thus reducing the loaded cavity uniformity. Hence, positions 5 and 8 are the most suitable for the double-ridged horn antenna to improve the average electromagnetic field intensity while maintaining a high uniformity.

Fig. 4(b) shows the probability density (histogram) of the normalized electric field for two selected scenarios (position 8 using the double-ridged horn antenna and the conical antenna). The x-axis represents the normalized electric field intensity relative to the mean, i.e., the zero point on the x-axis of the histogram represents the average electric field. We observe that the variability of the electric field using the conical antenna is higher than that with the horn antenna. Based on the obtained results, we select position 8 to run the RFAL experiments since it simultaneously provides high electromagnetic field uniformity and intensity. The spatial distribution of the electric field norm is shown in Fig. 4(c) (double-ridged horn antenna) and Fig. 4(d) (conical antenna). The electric field variability is lower using the horn antenna, whereas its average electric field is higher than that of the

TABLE II
FREEZE-DRYING PROCESS PARAMETERS FOR 4% w/v MANNITOL + 2% w/v SUCROSE IN 6R VIALS, WITH A FILL VOLUME OF 3 mL AND A DELIVERED RF POWER OF 25 W (8 GHz)

	Shelf Temperature Set-point	Ramp Time	Hold Time	Vacuum Set-point	Vials Size
Freezing	$-40°C$	120 Minutes	60 Minutes	760,000 mTorr	6R
Annealing	$-15°C$	50 Minutes	240 Minutes	760,000 mTorr	
Primary Drying	$10°C$	50 Minutes	CONV: 630 Minutes RF1: 350 Minutes RF2: 290 Minutes	70 mTorr	

conical antenna. Such behavior is attributed to the reduced RF waves absorbed by the horn antenna due to its high directivity. The spatial distributions cover the space inside the RC where the products are placed [highlighted in blue in Fig. 4(a)]. The box used to obtain the spatial electric field distribution is at least $\lambda/2$ away from all the metallic walls to avoid field nonuniformity [24], [31].

Unlike most previous studies on RF lyophilization processes, which rely on the ISM band (2.45 GHz), we used 8 GHz in this work. The primary drying time and electromagnetic field uniformity are improved at that particular frequency. The field uniformity increases inside the chamber by increasing the number of excited modes. For an arbitrary cavity with a particular volume, the smoothed number of modes according to Weyl's law is [32]

$$N_W(f) = \frac{8\pi V f^3}{3c^3} \tag{8}$$

where V represents the volume of the cavity, f is the frequency of operation, and c is speed of light. The rectangular cavity, on the other hand, reduces the degenerated modes to further improve the electric field uniformity.

The total absorbed RF power density by ice during the freeze-drying is obtained using

$$P_{\text{Absorbed}}(f) = 2\pi f \epsilon_0 \epsilon'' |\mathbf{E}|^2 \tag{9}$$

where ϵ_0 is the free-space permittivity, and ϵ'' represents the loss factor of ice, which is more than twice as high at 8 GHz compared with 2.45 GHz [33]. Hence, as the frequency of operation increases, the primary drying time of lyophilization becomes shorter.

III. FREEZE-DRYING EXPERIMENTAL SETUP

All the lyophilization cycles are conducted in a laboratory-scale lyophilizer (LyoStar3 from SP Scientific) in the LyoHub facility at the Birck Nanotechnology Center, Purdue University. Fig. 5 shows the experimental setup used. A conventional run that does not involve RF heating is initially conducted (reference cycle). Then, we carry out two additional cycles using the developed quasi-random field (qRF) system (i.e., using the conical antenna and the double-ridged horn antenna). The output RF signal of the power amplifier is set to 45 W to ensure that around 25 W reaches the antenna's port (2.5 dB insertion loss). To study the impact of field uniformity of the lyophilized products, a Metrohm 874 Karl Fischer Oven with 851 Coulometer

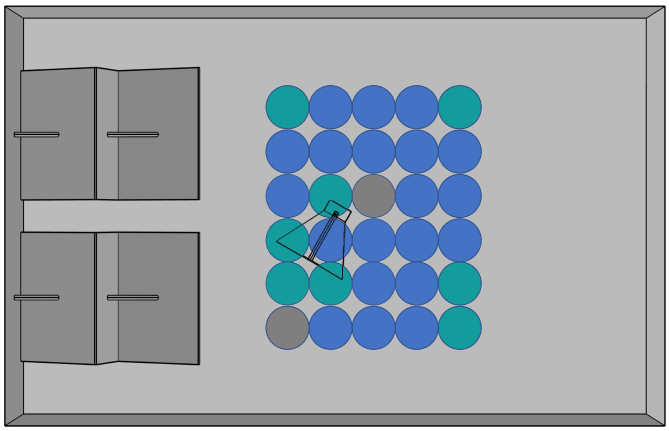

Fig. 7. Top view of the RF box with vials placement. Blue vials represent the vials used to obtain the moisture content of the three cycles.

moisture analyzer (Fig. 6) is used to determine the residual moisture content.

Table II summarizes the recipe used in the experiments. For every experiment, we used 20 samples to obtain the residual moisture content (shown in blue in Fig. 7). Optical temperature sensors monitor the product temperature of two samples (shown in gray in Fig. 7). In addition, we used annealing, a process step in which products are kept at a specific subfreezing condition above the transition temperature of the glass for a while. Such a step reduces the heterogeneity of the samples during the sublimation process [34], [35]. We did not perform the secondary drying to have a better insight into the impact that qRF has on residual moisture content of the lyophilized products.

IV. RESULTS AND DISCUSSION

The process data of the three freeze-drying cycles are shown in Fig. 8(a)–(c). The end of the primary drying is identified when the Pirani gauge (Vacuum P) and the capacitance manometer (CM) converge within a predetermined value. The CM sensor indicates the absolute pressure inside the chamber, whereas the Pirani gauge reads the pressure through the gas's thermal conductivity. Inside the freeze-dryer, nitrogen and water vapor gases exist during the primary drying phase. The water vapor, which has a higher thermal conductivity than nitrogen by about 60%, is a direct result of the sublimation. Nitrogen, on the contrary, is used to control the pressure inside the chamber. Hence, the Pirani gauge reading is about 60% higher than that of the CM when the water vapor is

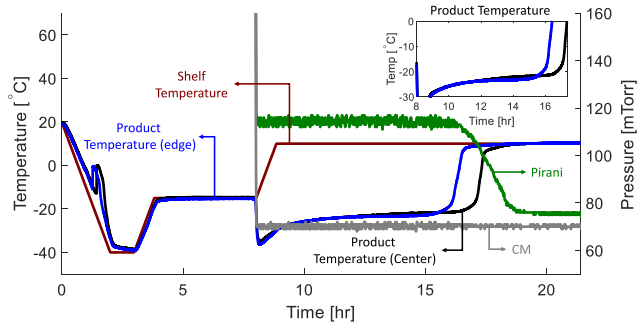

(a)

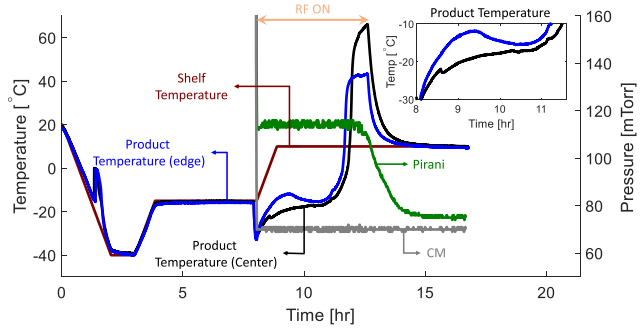

(b)

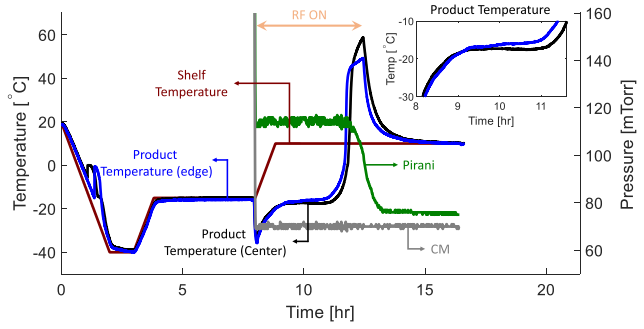

(c)

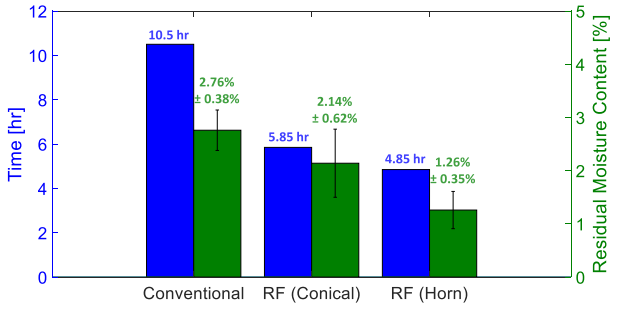

(d)

Fig. 8. Process data of (a) conventional lyophilization cycle, (b) RFAL cycle using the conical antenna, and (c) RFAL cycle using the double-ridged horn antenna. (d) Primary drying time and residual moisture content data (average +/− std) for the three cycles.

the dominant gas inside the chamber. The convergence of the Pirani gauge within a specified tolerance indicates the end of the primary drying phase [4]. The end of the primary drying in this work has been determined using the second derivative approach proposed in [36].

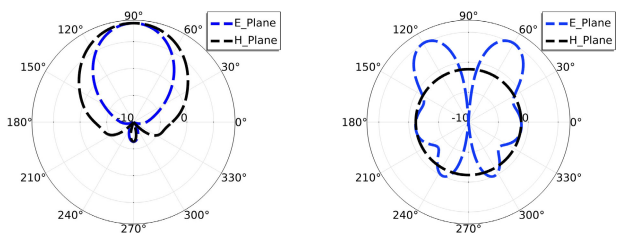

(a) (b)

Fig. 9. Simulated far-field radiation pattern of (a) double-ridged horn antenna and (b) wideband conical antenna.

Based on the obtained results, the electromagnetic field uniformity using the horn antenna is improved since it is directed toward the mechanical stirrers. Using an omnidirectional antenna (e.g., conical antenna) for such an application reduces the electromagnetic field uniformity (Fig. 9 shows the simulated radiation pattern of both the antennas at 8 GHz). The conical antenna exposes some of the products inside the chamber to RF waves before being scattered by the mechanical stirrers. Thus, the power density of the waves directed toward these vials is higher than that with the horn antenna. We observe a significant product temperature discrepancy between the products using the conical antenna, as shown in Fig. 8(b). Such a temperature variation is reduced when using the horn antenna since the mechanical stirrers scatter the field inside the chamber [Fig. 8(c)]. The residual moisture content for the three cycles verifies that batch homogeneity is significantly improved using the horn antenna as depicted in Fig. 8(d). It is also observed that the primary drying time is lowest with the horn antenna. Using a directive antenna for such an application reduces the reflected power back to the antenna, thus increasing the average electric field (as depicted in the simulation models).

qRF lyophilization outperforms the conventional lyophilization process in the primary drying acceleration and the average residual moisture content [as depicted in Fig. 8(d)]. The radiation heating mechanism involved with the RFAL at 8 GHz explains the observed speedup in the primary drying phase due to the increase in the absorbed RF power.

All the FE models in this study assumed an empty chamber to reduce the computational time associated with the addition of the products. Hence, variations in the electromagnetic field metrics are expected if such FE models consider the frozen product (i.e., loaded cavity). Nonetheless, by comparing the simulated and measured results, it is observed that the FE model results can be used along with the SEM theory to design such chambers for pharmaceutical lyophilization.

V. Conclusion

In this work, we have demonstrated the design of an RC using the SEM theory for pharmaceutical lyophilization, specifically using FE models. qRF lyophilization significantly improves efficiency by reducing the total drying time. The results obtained for freeze-drying of 4% w/v mannitol and 2% w/v sucrose showed an acceleration in primary drying time by 81% using the wideband conical antenna and 119% using the double-ridged horn antenna. The conical antenna

degrades the field uniformity due to the high power density received by the products closer to the antenna. On the other hand, if the horn antenna is placed closer to the metallic walls or the mechanical stirrers, the reflected signal absorbed by the antenna could be significant, thus reducing the average electromagnetic field intensity. The traditional freeze-drying relies heavily on conductive heat transfer from the shelf to the vials which is highly inefficient in the vacuum environment. In our experimental setup, we conduct comparative testing to evaluate the enhancement of heat transfer from the shelf through the application of RFAL, aiming to accelerate the drying process. Using the same shelf temperature, we can isolate and assess the effect of additional microwave heating. In addition, many recent practical applications of lyophilization such as dual-chamber syringes and beads do not use vials. In such applications, conventional freeze-drying faces additional limitations. RF heating, which heats the products volumetrically and uniformly, enables direct energy transfer to the products regardless of their position or direct contact with the shelf.

ACKNOWLEDGMENT

The authors would like to acknowledge the support from the Advanced Lyophilization Technology HUB—LyoHUB for the use of lyophilization equipment at the LyoHUB Technology Demo Facility at Purdue University. The content is solely the responsibility of the authors and does not necessarily represent the official views of NIIMBL. The RFAL technology development has been supported by the Elmore Family School of Electrical and Computer Engineering and by the Davidson School of Chemical Engineering, at Purdue University.

REFERENCES

[1] A. Alexeenko and E. Topp, *Future Directions: Lyophilization Technology Roadmap to 2025 and Beyond*. Hoboken, NJ, USA: Wiley, 2025, ch. 1, pp. 355–372, doi: 10.1002/9783527802104.ch15.

[2] S. Grassini, M. Parvis, and A. A. Barresi, "Inert thermocouple with nanometric thickness for lyophilization monitoring," *IEEE Trans. Instrum. Meas.*, vol. 62, no. 5, pp. 1276–1283, May 2013, doi: 10.1109/TIM.2012.2223312.

[3] M. Parvis, S. Grassini, and A. Barresi, "Sputtered thermocouple for lyophilization monitoring," in *Proc. IEEE Int. Instrum. Meas. Technol. Conf.*, May 2012, pp. 1994–1998, doi: 10.1109/I2MTC.2012.6229263.

[4] A. Abdelraheem et al., "Statistical electromagnetics for industrial pharmaceutical lyophilization," *PNAS Nexus*, vol. 1, no. 3, Jul. 2022, Art. no. pgac052.

[5] S. Grassini, D. Mombello, A. Neri, M. Parvis, and A. Vallan, "Plasma deposited thermocouple for non-invasive temperature measurement," in *Proc. IEEE Instrum. Meas. Technol. Conf.*, May 2009, pp. 732–736, doi: 10.1109/IMTC.2009.5168547.

[6] X. Jiang et al., "A non-invasive multipoint product temperature measurement for pharmaceutical lyophilization," *Sci. Rep.*, vol. 12, no. 1, Jul. 2022, Art. no. 12010.

[7] N. Raghunathan, X. Jiang, D. Peroulis, and A. Ganguly, "Wireless low-power temperature probes for food/pharmaceutical process monitoring," in *Proc. IEEE Sensors*, Nov. 2015, pp. 1–4, doi: 10.1109/ICSENS.2015.7370356.

[8] N. Raghunathan, X. Jiang, A. Ganguly, and D. Peroulis, "An ANT-based low-power battery-free wireless cryogenic temperature probes for industrial process monitoring," in *Proc. IEEE Sensors*, Oct. 2016, pp. 1–3, doi: 10.1109/ICSENS.2016.7808751.

[9] J. H. Gitter, R. Geidobler, I. Presser, and G. Winter, "Microwave-assisted freeze-drying of monoclonal antibodies: Product quality aspects and storage stability," *Pharmaceutics*, vol. 11, no. 12, p. 674, Dec. 2019.

[10] V. Gervasi, R. Dall Agnol, S. Cullen, T. McCoy, S. Vucen, and A. Crean, "Parenteral protein formulations: An overview of approved products within the European union," *Eur. J. Pharmaceutics Biopharmaceutics*, vol. 131, pp. 8–24, Oct. 2018, doi: 10.1016/j.ejpb.2018.07.

[11] A. Bhambhani and J. T. Blue, "Lyophilization strategies for development of a high-concentration monoclonal antibody formulation: Benefits and pitfalls," *Amer. Pharmaceutical Rev.*, vol. 13, no. 1, pp. 31–38, 2010.

[12] A. Bhambhani et al., "Evaluation of microwave vacuum drying as an alternative to freeze-drying of biologics and vaccines: The power of simple modeling to identify a mechanism for faster drying times achieved with microwave," *AAPS PharmSciTech*, vol. 22, no. 1, pp. 1–16, Jan. 2021.

[13] T. Fauster, M. Giancaterino, P. Pittia, and H. Jaeger, "Effect of pulsed electric field pretreatment on shrinkage, rehydration capacity and texture of freeze-dried plant materials," *LWT*, vol. 121, Mar. 2020, Art. no. 108937, doi: 10.1016/j.lwt.2019.108937.

[14] S. Corbellini, M. Parvis, and A. Vallan, "In-process temperature mapping system for industrial freeze dryers," *IEEE Trans. Instrum. Meas.*, vol. 59, no. 5, pp. 1134–1140, 2010.

[15] A. I. Liapis, M. L. Pim, and R. Bruttini, "Research and development needs and opportunities in freeze drying," *Drying Technol.*, vol. 14, no. 6, pp. 1265–1300, Jan. 1996.

[16] T. T. Mutukuri, A. Darwish, A. D. Strongrich, D. Peroulis, A. Alexeenko, and Q. Zhou, "Radio frequency–assisted ultrasonic spray freeze drying for pharmaceutical protein solids," *J. Pharmaceutical Sci.*, vol. 112, no. 1, pp. 40–50, Jan. 2023.

[17] S. Ambros, R. Mayer, B. Schumann, and U. Kulozik, "Microwave-freeze drying of lactic acid bacteria: Influence of process parameters on drying behavior and viability," *Innov. Food Sci. Emerg. Technol.*, vol. 48, pp. 90–98, Aug. 2018.

[18] D. A. Copson, "Microwave sublimation of foods," *Food Technol.*, vol. 12, no. 6, pp. 270–272, 1958.

[19] J. P. Dolan, "Microwave freeze-drying of aqueous solutions," M.S. thesis, Mech. Eng., Virginia Tech, Blacksburg, VA, USA, 1994.

[20] W. Wang and G. Chen, "Freeze drying with dielectric-material-assisted microwave heating," *AIChE J.*, vol. 53, no. 12, pp. 3077–3088, 2007, doi: 10.1002/aic.11336.

[21] S. S. de Jesus and R. M. Filho, "Optimizing drying conditions for the microwave vacuum drying of enzymes," *Drying Technol.*, vol. 29, no. 15, pp. 1828–1835, Dec. 2011, doi: 10.080/07373937.2011.605977.

[22] J. H. Gitter, R. Geidobler, I. Presser, and G. Winter, "Significant drying time reduction using microwave-assisted freeze-drying for a monoclonal antibody," *J. Pharmaceutical Sci.*, vol. 107, no. 10, pp. 2538–2543, Oct. 2018.

[23] A. M. M. Abdelraheem, M. D. Sinanis, and D. Peroulis, "Rf-heating in industrial metallic chambers," U.S. Patent 16 587 151, Feb. 11, 2021.

[24] Q. X. Huang, *Fundamentals Reverberation Chamber*. Hoboken, NJ, USA: Wiley, 2018, ch. 5, pp. 89–131, doi: 10.1002/9781119362050.ch5.

[25] B. H. Liu, D. C. Chang, and M. T. Ma, "Eigenmodes and the composite quality factor of a reverberatingchamber," U.S. Dept. Commerce, Malcolm Baldrige, Secretary, Tech. Note (NIST TN)—1066, Aug. 1983.

[26] D. A. Hill, "Plane wave integral representation for fields in reverberation chambers," *IEEE Trans. Electromagn. Compat.*, vol. 40, no. 3, pp. 209–217, Aug. 1998.

[27] (2022) Frequency selective surface, periodic complementary split ring resonator. https://www.comsol.com/model/frequency-selective-surface-periodic-complementary-split-ring-resonator-15711

[28] *Electromagnetic Compatibility (EMC)—Part 4–21: Testing and Measurement Techniques—Reverberation Chamber Test Methods*, document IEC 61000-4-21:2011, Geneva, Switzerland, Jan. 2011.

[29] B. Dmoulin and P. Besnier, *Statistical Behavior of Stirred Waves in an Oversized Cavity*. Hoboken, NJ, USA: Wiley, 2011, ch. 3, pp. 83–133.

[30] A. Darwish, M. D. Sinanis, and D. Peroulis, "Design of a reverberation chamber for lyophilization: Finite-element based approach," in *Proc. IEEE Int. Symp. Antennas Propag. USNC-URSI Radio Sci. Meeting (AP-S/URSI)*, Jul. 2022, pp. 1850–1851, doi: 10.1109/AP-S/USNC-URSI47032.2022.9887079.

[31] D. A. Hill, *Electromagnetic Fields in Cavities: Deterministic and Statistical Theories*. Hoboken, NJ, USA: Wiley, 2009.

[32] W. Strauss, *Partial Differential Equations: An Introduction*. Hoboken, NJ, USA: Wiley, 2007. [Online]. Available: https://books.google.com/books?id=m2hvDwAAQBAJ

[33] T. Matsuoka, S. Fujita, and S. Mae, "Effect of temperature on dielectric properties of ice in the range 5–39 GHz," *J. Appl. Phys.*, vol. 80, no. 10, pp. 5884–5890, Nov. 1996, doi: 10.1063/1.363582.

[34] J. A. Searles, J. F. Carpenter, and T. W. Randolph, "Annealing to optimize the primary drying rate, reduce freezing-induced drying rate heterogeneity, and determine T'g in pharmaceutical lyophilization," *J. Pharmaceutical Sci.*, vol. 90, no. 7, pp. 872–887, Jul. 2001, doi: 10.1002/jps.1040.

[35] W. Abdelwahed, G. Degobert, and H. Fessi, "Freeze-drying of nanocapsules: Impact of annealing on the drying process," *Int. J. Pharmaceutics*, vol. 324, no. 1, pp. 74–82, Oct. 2006, doi: 10.1016/j.ijpharm.2006.06.047.

[36] A. Hanama, R. Kinoshita, T. Kodama, and N. Nishimoto, *Lyophilization Study With μ-CT and Pirani Vacuum Gauge*, Daiichi Sankyo Co., Tokyo, Japan, 2021.

Ahmad Darwish (Member, IEEE) received the B.S. degree from the American University of Sharjah, United Arab Emirates, in 2016, and the M.Eng. and Ph.D. degrees in electrical engineering from Texas A&M University, College Station, TX, USA, in 2018 and 2021, respectively.

He is a Senior Research Associate at the Elmore Family School of Electrical and Computer Engineering, Purdue University, West Lafayette, IN, USA. From 2021 to 2022, he was a Post-Doctoral Research Assistant at Purdue University. He has coauthored more than 20 journal and conference papers and is a co-inventor of three patents. His research interests include span RF-assisted lyophilization, high-power antenna and microwave passive devices' design, ultrahigh-frequency (UHF)-based partial discharge detection, microwave/RF heating, PCB design, and RF ICs integration.

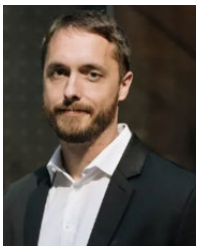

Andrew David Strongrich received the Ph.D. degree from the School of Aeronautics and Astronautics, Purdue University, West Lafayette, IN, USA, in 2021, with a focus on industrial wireless sensor networks and technologies.

He is a Research Scientist at LyoHub, an industry-driven consortium at Purdue University, with 32 member companies that span the global pharmaceutical freeze-drying ecosystem. His current research interests include microwave-assisted freeze-drying, computational modeling, and design, fabrication, and testing of novel process analytical technologies.

Alina Alexeenko received the Ph.D. degree in aerospace engineering from Pennsylvania State University, State College, PA, USA, in 2003.

She was a WiSE Post-Doctoral Fellow at the University of Southern California, Los Angeles, CA, USA, from 2004 to 2006. She is a Professor at the School of Aeronautics and Astronautics and Davidson School of Chemical Engineering. She is currently the Senior Associate Dean with the College of Engineering, Purdue University, West Lafayette, IN, USA. She has authored more than 200 journal and conference papers and is a co-inventor of ten patents. She has been collaborating broadly with industry firms on design and improvement of pharmaceutical lyophilization equipment and processes since 2008 and co-led the development of LyoHUB's Lyophilization Technology Roadmap to 2025 and Beyond and the first recognized consensus technical standard for pharmaceutical lyophilization issued by ASTM in 2022. She is a Founding Co-Director of Advanced Lyophilization Technology Hub—LyoHUB established in 2014 focused on advancing the science and technology of pharmaceutical lyophilization for manufacture biopharmaceuticals and vaccines. Her research interests include rarefied gas dynamics, heat and mass transfer process modeling in application to high-altitude aerothermodynamics and spacecraft technologies, and pharmaceutical manufacturing.

Dr. Alexeenko is an Associate Fellow of the American Institute of Aeronautics and Astronautics (AIAA) and served as the Chair for the AIAA Thermophysics Technical Committee from 2016 to 2018.

Dimitrios Peroulis (Fellow, IEEE) received the Ph.D. degree in electrical engineering from the University of Michigan at Ann Arbor, Ann Arbor, MI, USA, in 2003.

He is the Senior Vice President for Purdue University Online and the Reilly Professor of the Elmore Family School of Electrical and Computer Engineering at Purdue University, West Lafayette, IN, USA. From 2019 to 2023 he served as the Michael and Katherine Birck Head of ECE and Special Adviser to the Dean of Engineering on online learning. He has coauthored more than 450 journal and conference papers. His research interests are focused on the areas of reconfigurable systems, plasma RF electronics, and RF-assisted lyophilization. He has been a key contributor in developing high-quality widely tunable filters and novel filter architectures based on miniaturized high-Q cavity-based resonators.

Dr. Peroulis received the National Science Foundation CAREER award in 2008. In 2019, he received the "Tatsuo Itoh" Award, and in 2014 he received the Outstanding Young Engineer Award both from the IEEE Microwave Theory and Techniques Society (MTT-S). In 2012, he received the Outstanding Paper Award from the IEEE Ultrasonics, Ferroelectrics, and Frequency Control Society (Ferroelectrics section). His students have received numerous student paper awards and other student-research-based scholarships. He has been a Purdue University Faculty Scholar and has also received 11 teaching awards including the 2010 HKN C. Holmes MacDonald Outstanding Teaching Award and the 2010 Charles B. Murphy award, which is Purdue University's highest undergraduate teaching honor.